Published in final edited form as:
Radiat Res. 2013 April ; 179(4): 465–474. doi:10.1667/RR3127.1.

Enalapril Mitigates Focal Alveolar Lesions, A Histological Marker of Late Pulmonary Injury by Radiation to the Lung

Feng Gao[a,1], **Jayashree Narayanan**[a], **Cortney Joneikis**[b], **Brian L. Fish**[a], **Aniko Szabo**[c], **John E. Moulder**[a], **Robert C. Molthen**[b,g,h], **Elizabeth R. Jacobs**[b,d,f,g], **R. Nagarjun Rao**[e], and **Meetha Medhora**[a,b,d,f,g]

[a]Department of Radiation Oncology, Medical College of Wisconsin, Milwaukee, Wisconsin

[b]Department of Medicine, Medical College of Wisconsin, Milwaukee, Wisconsin

[c]Institute for Health and Society, Division of Biostatistics, Medical College of Wisconsin, Milwaukee, Wisconsin

[d]Department of Physiology, Medical College of Wisconsin, Milwaukee, Wisconsin

[e]Department of Pathology, Medical College of Wisconsin, Milwaukee, Wisconsin

[f]Cardiovascular Center, Medical College of Wisconsin, Milwaukee, Wisconsin

[g]Research Service, Department of Veteran's Affairs, Zablocki Veterans Affairs Medical Center, Milwaukee, Wisconsin

[h]Department of Biomedical Engineering, Marquette University, Milwaukee, Wisconsin

Abstract

The goal of our study was to identify a histological marker for testing countermeasures for mitigation of late radiation injury to the lung. Pulmonary fibrosis is currently the best described "late effect" in survivors of acute radiation pneumonitis. However, robust fibrosis does not develop in some rodent strains for years after a single dose of radiation to the whole thorax. We observed radiation-associated focal alveolar lesions that were rich in giant cells and macrophages containing cholesterol clefts in the lungs of irradiated WAG/ RijCmcr rats. These lesions were first observed after pneumonitis, around 21 weeks after receiving a radiation dose of 13 Gy to the thorax but not until 71 weeks in unirradiated rats. The number of cholesterol clefts increased with time after irradiation through 64 weeks of observation, and at 30 weeks after 13 Gy, cholesterol clefts were associated with several indices of deterioration in lung function. The number of cholesterol clefts in irradiated lung sections were reduced by the angiotensin converting enzyme (ACE) inhibitor enalapril (25–42 mg/m^2/day) from 18.7 ± 4.2/lung section to 6.8 ± 2.4 (P = 0.029), 5.2 ± 1.9 (P = 0.0051) and 6.7 ± 1.9 (P = 0.029) when the drug was started at 1 week, 5 or 15 weeks after irradiation, respectively, and continued. Similar lesions have been previously observed in the lungs of one strain of irradiated mice and in patients following radiotherapy. We propose that alveolar lesions with cholesterol clefts may be used as a histological marker of the severity of radiation lung injury and to study its mitigation in WAG/

[1]Address for correspondence: MFRC 6030, Radiation Oncology, Medical College of Wisconsin, 8701 Watertown Plank Road, Milwaukee, Wisconsin 53226; fgao@mcw.edu.

INTRODUCTION

The lung is a sensitive target of irradiation. It is well known that single or fractionated doses of X or γ rays above 8 Gy induce two phases of injury, an acute pneumonitis that usually manifests after 6 weeks and fibrosis that starts from months to years later (1–4). A number of reports suggest that radiation-induced pulmonary fibrosis may be regulated by genetic (5–7) and other factors such as the dose of radiation (8). Fibrosis is defined as scarring due to the accumulation of collagen. It is identified *in vitro* by histological staining and/or biochemical assays for increase in tissue collagen, a protein that is difficult to solubilize and that is also abundant in larger airways and blood vessels of the normal lung. Other late effects of radiation in the lung are less well described, and even though fibrosis is difficult to quantitate and can take months or years to develop after exposure to radiation, it is currently the standard marker of radiation-induced late effects in the lung.

Studies in C3H mice described focal granulomatous nodules 15 months after radiation exposure to the thorax given as split doses 28 days apart (9). Fractionation spared mortality due to pneumonitis, but did not alter the late effects in the lung. In this model, the breathing rate of mice increased after 15 months and this increase was reduced by injection of the radioprotector WR-2721, a thiol S-2-(3-aminopropylamino)-ethylphosphorotahcioic acid (now known as amifostine or Ethyol). Pretreatment with WR-2721 improved survival of irradiated mice. The lethal dose at which half the animals were alive (LD_{50}) at 15 months was increased from 8.63 Gy to 13 Gy. However, the drug treatment resulted in increased lung collagen as measured by assaying hydroxyproline, a marker specific for collagen. Thus, lung dysfunction and lethality induced by irradiation did not correlate with pulmonary fibrosis. The most striking change in this late stage was the presence of focal scars. Travis *et al.* (9), state that the scars were made up of a “collection of lymphocytes in the interstitium, accompanied by ‘foamy’ cells in the alveolar spaces and collagen deposits in the area forming a focal scar. Empty, long needle-like crystalline spaces resembling cholesterol clefts were observed in these scarred areas. Histological evidence of collagen was present in these areas only and was not observed in the interstitium of the alveoli”. In that study signs of pneumonitis that had occurred earlier were absent (9). No detailed immunological characterization of the cells in the lesions or in the development with time after irradiation were described in these studies. Furthermore, WR-2721 did not protect the lung from radiation fibrosis.

We have demonstrated an increase (doubling) in lung collagen at 30 weeks (7 months) after a single dose of 13 Gy of X rays to the whole thorax of WAG/RijCmcr rats. In addition, we demonstrated that this effect was mitigated by the ACE inhibitors, enalapril, captopril and fosinopril (10). Two of these drugs (captopril and enalapril) improved survival during pneumonitis between 6–10 weeks. Histological analysis of lung sections at 30 weeks revealed scattered lesions consisting of intra-alveolar collections of foamy macrophages, many of which contained cholesterol cleft-like structures, similar to those described above by Travis *et al.* (9, 11, 12).

The purpose of the current study was to develop a quantitative, histological biomarker to investigate mitigators of late effects of radiation to the lung. For these investigations we used our model of mature female WAG/ Rij rats that has been well characterized by us and others and shown to be sensitive to radiation injury in the lungs (10, 13–16). We showed that these rats (>60%) were lost to morbidity due to pneumonitis after receiving a radiation dose of 13 Gy to the whole thorax, and that collagen synthesis in the lung was increased in survivors after 30 weeks, but not 26 weeks, indicating onset of pulmonary fibrosis (10). The WAG/Rij rats are descendants of an inbred strain originally created by A. L. Bacharach in 1924 from outbred Wistar rats and maintained by Glaxo laboratories in the UK. They were

housed at the Radiological Institute of The Netherlands before they were brought to the U.S. The WAG/RijCmcr rats at the Medical College of Wisconsin were originally derived from a Yale University colony (17).

In the current study, we used WAG/RijCmcr rats to: (1) evaluate histology of alveolar lesions in irradiated lungs; (2) examine the relationship between cholesterol cleft density and time elapsed after irradiation; (3) estimate the relationship between cholesterol cleft density after increasing doses of radiation and measure changes in lung structure, vasculature and function at the same times; (4) evaluate the association of the intra-alveolar lesions with fibrosis; and (5) determine if the ACE inhibitor enalapril, which is known to mitigate pulmonary fibrosis, also mitigates the intra-alveolar lesions.

MATERIALS AND METHODS

Animal Care

The study was approved by the Institutional Animal Care and Use Committee (IACUC) at the Medical College of Wisconsin. Female rats (WAG/RijCmcr) were housed in a moderate security barrier. Based upon directives from the IACUC of the Medical College of Wisconsin, rats were considered morbid and euthanized if they met specified veterinarian's criteria. These included at least 3 of the following: (1) greater than 20% loss in body weight, (2) inactivity on 2 consecutive days, defined as no movement unless actively stimulated, (3) lack of grooming that became worse after 24 h, (4) breathing rates of less than 60 or greater than 250 breaths per minute and (5) hunched posture or death pose on 2 consecutive days.

Injury Models

Unanesthetized 9- to 10-week-old rats weighing approximately 140 g were immobilized in a plastic jig and were irradiated with a 320-kVp orthovoltage system X rays with a half-value layer (HVL) of 1.4 mm Cu (15). Rats were treated with a single dose of 5–13 Gy to the whole thorax at a dose rate of 1.43 Gy/min (10). The radiation dose was delivered by two equally weighted lateral beams to improve uniformity. The whole lung, heart and a small amount of liver were in the field. The irradiated rats and their age-matched controls were sacrificed at different times from 20–71 weeks after irradiation. The lungs were harvested and processed for histopathology.

Administration of Drug

Random selected animals were treated with enalapril (gift from Merck Inc. or catalogue no. E6888, Sigma Chemicals, St. Louis, MO) added to the drinking water (30 and 60 mg/L), as described by us and others (10, 14, 18–20). As previously reported, this concentration delivers 12.5–42 mg/m^2/day (1 standard deviation above and below the mean). The drug was started at 1, 5, 10, 15 or 20 weeks after irradiation and continued until the study was terminated at 30 weeks.

Histology

The whole or partial lung was removed at sacrifice, fixed in 10% neutral buffered formalin (Fisher Scientific, Pittsburg, PA) and embedded in paraffin. Whole-mount sections of the left lung were cut (4 μm), processed and stained with Hematoxylin & Eosin (H&E, Richard Allan, Kalamazoo, MI) or Masson's Trichrome (Newcomer Supply, Middleton, WI). Some partial lung sections were also processed in the same manner. All mounting, paraffin embedding and staining were performed by the Children's Research Institute-Histology Core at the Medical College of Wisconsin.

Immunohistochemistry

Sectioning and staining for myeloperoxidase, tryptase, CD31, keratin-7 and actin is detailed in Table 1. As described previously (21), formalin-fixed, paraffin-embedded longitudinal 4 μm sections of the whole-mount left lung were deparaffinized followed by antigen retrieval in citrate buffer pH 6 for a total of 40–60 min. Endogenous peroxide activity was quenched by incubating the samples in 3% H_2O_2. Samples were incubated at room temperature with the optimized dilutions of primary antibodies as shown in Table 1. Incubation time was 60 min for all of the antibodies except for keratin-7, which was incubated overnight. For detection, horseradish peroxidase (HRP)-conjugated secondary antibodies and a peroxidase-based system [labeled streptavidin biotin method (LSAB)] were used for signal amplification. Mayer's hematoxylin was used as the counterstain.

Sectioning and staining for CD 68, CD 43 and CD 79a as detailed in Table 1 were performed by the Physiology Histology Laboratory at the Medical College of Wisconsin following a similar procedure as described above, except that Vector biotinylated secondary antibodies and Elite ABC kit (Dako Laboratories, Carpintaria, CA) were used for detection. Aniline blue was used as the counterstain. At both staining facilities, appropriate positive and negative controls with relevant histological tissue sections were included for each stain to ensure specificity of the signal.

Quantification of Staining in Lung Sections

All lung sections stained with H&E or Masson's trichrome were reviewed independently by two investigators who were blinded to the treatment groups. We quantified the number of cholesterol clefts/ whole-mount area of the left lung in cellular lesions containing at least 2 visible clefts with characteristic needle-shaped spaces (Fig. 1A) at the same magnification. A few partial-lung sections were included for time point studies. In these cases, the area of each section was individually traced and measured using ImageJ software and the corresponding number of cholesterol clefts were calculated and expressed for an average area covered by the whole-mount section from the left lungs. Only whole mount and not partial sections of the left lung at 30 weeks after irradiation were used for counting cholesterol clefts in the studies comparing animals not treated with drugs to those given different schedules of enalapril.

Measurement of Breathing Rate, Lung Collagen, Body Weight, Total Lung ACE Activity, Right Ventricular Hypertrophy, Pulmonary Vascular Resistance, Dry Lung Weight and Pulmonary Arterial Distensibility

These end points were measured in rats at different times after doses of 5, 10 and 13 Gy to the thorax, as shown in Table 2. The techniques were performed as described by us previously as follows: breathing rate (15), newly synthesized lung collagen by the Sircol assay (10, 16) and body weight (22). Total lung angiotensin converting enzyme (ACE) activity, pulmonary vascular resistance, right ventricular hypertrophy, dry lung weight and pulmonary arterial distensibility were measured in isolated and perfused lungs *ex vivo*, as detailed by Ghosh *et al.* (22).

Statistical Analysis

Average numbers of cholesterol clefts/whole mount area/group were compared by one-way analysis of variance (ANOVA). Bar graph values are expressed as mean ± SEM (stand error of the mean). In studies comparing only 2 groups (morphometric ratios of staining from cellular lesions versus lung parenchyma and irradiation versus irradiation with all schedules of enalapril), *t* tests were used. To examine the increase in cholesterol clefts with time and drug, the data were square root transformed to stabilize the variance (23). An examination of

the residuals in a one-way ANOVA confirmed the appropriateness of the transformation. A trend test was performed by using a linear regression model with equally spaced scores for the time variable. One-way ANOVA was followed by either Tukey's HSD (Honestly Significant Differences) procedure for pairwise comparison of all group means, Dunnett's procedure for comparison to a control group (13 Gy, no drug) or the Holm-Sidak method when permitted.

RESULTS

Histological Analysis of Alveolar Lesions

Lungs were harvested between 21–71 weeks after radiation doses of 13 Gy to the thorax and studied after histological processing. Typical cellular foci with alveoli containing cholesterol clefts were carefully examined in these lungs as described below.

1. Staining with H&E—Lung sections stained with H&E (Fig. 1A) demonstrated inflammatory cellular foci (see alveolar lesion in the left panel) mainly in peribronchiolar regions surrounded by more normal lung parenchyma (right panel). The alveolar framework within these foci was loosely visible but the air spaces were filled by foamy macrophage exudates similar to lesions observed in diffuse pan bronchiolitis (DPB). The coalesced histiocytes formed multinucleate giant cells with lipoid material (cholesterol clefts). The cholesterol clefts were visualized as long needle-shaped spaces (marked with arrows) (24), with no inclusions defined by polarized light either inside or outside the giant cells. A related change in the parenchyma was the presence of foci with peribronchiolar metaplasia (see the arrows in Fig. 1B).

2. Staining with Masson's Trichrome—The trichrome stain highlighted collagen deposition (blue staining) associated with intra-alveolar foci containing foamy macrophages (Fig. 1C, left panel). The fibrotic foci were seen as thickenings of alveolar walls compared to the adjacent lung parenchyma shown in Fig. 1C (right panel). Morphometric comparisons were made of the ratio of red (noncollagenous) versus blue (collagenous) stain in a single lesion (example shown in the circle in Fig. 1C) in each of 8 rat lungs, versus 2 random areas of parenchyma in each of the same lung sections (e.g., Fig. 1C, right panel). This ratio decreases with increased fibrosis. Parenchymal regions were chosen remote from large vessels or airways, structures that are known to contain collagen in normal lungs. There was no difference between the mean red:blue ratios from the lesions when compared to the ratio in the parenchyma, as shown in the graph (Fig. 1D).

3. Immunohistochemistry (IHC) Staining

Anti-ED-1 (CD68): This immunostain highlights macrophages. A stained whole-mount lung section was scanned under low magnification to show macrophage-rich foci predominantly in perivascular or peribronchiolar locations (see arrows in Fig. 1E). In contrast, the surrounding parenchyma showed only occasional macrophages within the alveolar spaces. Under higher magnification, these histiocytes were heavily stained with ED-1 (Fig. 2A, brown stain in the left panel) again indicating aggregates of macrophages compared to the surrounding parenchyma (Fig. 2A, right panel).

Anti-myeloperoxidase: This immunostain also abundantly marked the macrophages (Fig. 2B). Though there was staining of neutrophils that were sparsely interspersed in the parenchyma, myeloperoxidase was observed to localize within macrophages in the alveolar lesions. Closer examination and comparison with H&E sections by a pulmonary pathologist (NR) confirmed staining of macrophages with only a few neutrophils being present within the foci (Fig. 2B).

Anti-CD43 and CD79a: These markers for T and B lymphocytes, respectively, showed only a few cells scattered within the lesions as well as within the parenchyma. More T cells (Fig. 2C) seemed visible than B cells (Fig. 2D). There was no specific association or enrichment of either lymphocyte type within the lesions.

Anti-tryptase: Staining with this antibody highlighted the mast cells. Mast cells (stained brown) were uniformly present in the lesions as well as in the surrounding parenchyma (Fig. 2E).

Anti-CD-31: This immunostain was used to visualize the vascular endothelial cells. Alveolar lesions demonstrated small vessels (see arrow in Fig. 2F) that appeared to be squeezed by the surrounding giant cells and widening septa.

Keratin-7: This immunostain was used to mark epithelial cells (Fig. 2G). Similar to the endothelial cells, epithelial cells were compressed within the cellular lesions but characteristically lined adjacent open airways and surrounding parenchymal tissue.

Anti-alpha-smooth muscle actin: The bronchioles and arterioles were both positive for smooth muscle actin, which was localized within the lesions as well as in the parenchyma. A few clusters of positive cells were found surrounding the giant cells and the cholesterol clefts, as shown in Fig. 2H.

Alveolar Lesions in the Lung Increase with Time after Irradiation

We did not find cholesterol cleft-associated alveolar lesions in the lungs of unirradiated rats (0 Gy) corresponding to times at 30, 43 or 57 weeks after irradiation. The results are plotted in Fig. 3 (open circles). A small number of cholesterol clefts were observed in 4/6 unirradiated rats around 71 weeks, which averaged 4.78 ± 2.46 (mean ± SEM, $n = 6$) clefts in each whole-mount lung section (Fig. 3, open circles).

Rats irradiated with doses of 13 Gy to the whole thorax had increasing numbers of cholesterol clefts in lungs with time up to 64 weeks (Fig. 3, solid circles). Cholesterol cleft counts/whole-mount area were obtained from the lungs of 36 animals sacrificed at 21, 25, 30, 43 or 64 weeks. A line plot joining the mean value of the data is shown in Fig. 3. All pairwise comparisons between groups were significant by ANOVA (Tukey's test, see Materials and Methods section), except between 21 and 25 weeks. An increasing trend of cholesterol cleft counts with time was found ($P < 0.0001$).

Increasing Doses of Radiation Decrease Time to Develop Alveolar Lesions but Increase Numbers of Cholesterol Clefts

We counted cholesterol clefts in lungs irradiated with 5 Gy at 56 weeks, 10 Gy at 53 weeks and 12 Gy at 33 and 41 weeks. The results in Fig. 4 show no clefts after doses of 5 Gy at 56 weeks (open triangles) or 12 Gy at 33 weeks (open stars). There were comparable numbers of clefts after doses of 10 Gy at 53 weeks (solid triangles) or 12 Gy at 41 weeks (open stars), but these were lower than the numbers counted after a dose of 13 Gy at 30 or 43 weeks (Fig. 3, closed circles).

Presence of Alveolar Lesions is Associated with Other Structural and Functional Determinants of Lung Injury

Table 2 summarizes results of 8 assays connected with lung structure and function along with the number of cholesterol clefts/whole-mount sections observed at the same time after irradiation. Results for breathing rate, body weight, lung ACE activity, right ventricular hypertrophy, pulmonary vascular resistance, dry lung weight and arterial distensibility after

irradiation with 5 and 10 Gy have been described and presented in previous studies (15, 22). An increase in breathing rate and lung collagen after irradiation with 13 Gy has also been reported (10, 16). Results (mean ± SEM) for other assays (22) after 13 Gy and unirradiated rats (parallel controls), respectively, are as follows: body weight, 186 ± 3 and 201 ± 4 g (n = 8/group), P = 0.007; lung ACE activity, 7.4 ± 0.6 (n = 10) and 12.8 ± 0.3 units (n = 9), P < 0.001; right ventricular hypertrophy (ratio of weights of right ventricle: left ventricle + septum), 0.28 ± 0.02 (n = 10) and 0.21 ± 0.01 (n = 9), P = 0.003; pulmonary vascular resistance, 0.106 ± 0.005 (n = 10) and 0.086 ± 0.002 mmHg*min*kg/ml (n = 9), P = 0.005; dry lung weight, 0.0013 ± 0.00005 and 0.0008 ± 0.00002 (n = 8/group), P < 0.001; and arterial distensibility, 0.014 ± 0.001 (n =9) and 0.033 ± 0.001/mmHg (n =8), P < 0.001. As shown in Table 2, only one of 6 assays showed dysfunction at 56 weeks after irradiation with 5 Gy when compared to unirradiated controls. No cholesterol clefts were observed in these lungs. A total of four of 7 assays indicated dysfunction at 53 weeks after irradiation with 10 Gy. Lungs from these rats contained alveolar lesions with cholesterol clefts. After doses of 13 Gy at 30 weeks, eight of 8 assays showed pulmonary dysfunction and these lungs were associated with the highest number of clefts from the 3 groups.

Mitigation by the ACE Inhibitor Enalapril

Enalapril was started at five different time points (1, 5, 10, 15 and 20 weeks) after doses of 13 Gy to the thorax, and continued until the lungs were harvested at 30 weeks. The drug was given orally at 30 or 60 mg/L in the drinking water corresponding to a range of 12.5–42 mg/m^2/day. Body weights of the rats given enalapril (both doses) did not catch up to those of unirradiated rats at 30 weeks, but were also not different from irradiated rats with no drug (Fig. 5). There was no difference in body weight in rats given the high dose (60 mg/L) versus the low dose (30 mg/L) of drug even after 25 weeks of treatment with enalapril. We also did not observe differences in general indices of toxicity, including lack of grooming, inactivity, etc., in rats treated with enalapril versus their untreated counterparts.

At 30 weeks after a radiation dose of 13 Gy there were no cholesterol clefts in unirradiated lung sections, while lungs irradiated with 13 Gy had increased clefts (18.7 ± 4.2 clefts/whole-mount section, mean ± SEM, P = 0.0001, 13 Gy vs. 0 Gy) (Fig. 6). Results of ANOVA by Dunnett's procedure showed that three of the 5 schedules of enalapril (60 mg/L) mitigated the formation of cholesterol clefts after irradiation, starting at 1 week (6.8 ± 2.4, P = 0.029 vs. 13 Gy only), 5 weeks (5.2 ± 1.9, P = 0.0051 vs. 13 Gy only) and 15 weeks (6.7 ± 1.9, P = 0.029 vs. 13 Gy only). There were 8.6 ± 2.3 and 10.7 ± 3.9 clefts/whole-mount section when enalapril was started after 10 and 20 weeks, respectively. Lower doses of enalapril (30 mg/L) also mitigated formation of cholesterol clefts after irradiation when the drug was started after pneumonitis at 10 weeks (4.9 ± 1.9, P = 0.006 vs. 13 Gy only) and 20 weeks (7.3 ± 2.3, P = 0.029 vs. 13 Gy only). We could not compare results in groups in which the drug was started before pneumonitis due to <4 rats surviving in each of these groups. However, a t test comparing 13 Gy (n =8) to 13 Gy + enalapril 60 mg/L (n =40 by combining all groups) or 13 Gy + enalapril 30 mg/L (n = 32 by combining all groups) confirmed mitigation by the drug if started from 1–20 weeks after irradiation (P < 0.001 for 60 mg/L and P = 0.002 for 30 mg/L enalapril).

DISCUSSION

Radiation induces late focal alveolar lesions in rat lungs. The foci are predominantly peribronchial in location. This characteristic histopathology was first observed following pneumonitis, but before fibrosis was detected by measuring lung collagen (10). The cellular nodules are laden with lipoid-rich (foamy) multinucleate giant cells derived from macrophages that fill the alveolar space. The foci also contain a few lymphocytes and mast cells, although these were not markedly enhanced within the lesions compared to the

surrounding parenchyma. The alveolar septa within the lesions appeared thickened, though the collagen content in the lesion was not increased in proportion to the cellular density (Fig. 1C, D). The cholesterol clefts increased in number versus time up to 64 weeks, the longest time we observed. Cholesterol clefts appear earlier after doses of 13 Gy, than after irradiation with 12 or 10 Gy, and clefts were not present at 56 weeks after doses of 5 Gy. We observed the most indices of dysfunction in the lung and pulmonary vasculature of rats from the group containing the highest numbers of cholesterol granulomas. The numbers of clefts were reduced by therapy with enalapril started after thoracic irradiation. We did not measure the plasma levels of enalapril, drinking patterns over time or specific side effects of the drug, but did not observe general signs of toxicity in rats after any dose or schedule of enalapril we tested. Body weights of survivors of the pneumonitis phase measured at 30 weeks were identical in rats irradiated with dose of 13 Gy alone and to those also receiving enalapril in the water in schedules starting 1–20 weeks after irradiation. ACE inhibitors such as captopril, lisinopril and ramipril have been previously reported to mitigate a range of radiation-induced injuries in the lung and other organs (14, 25–29) and are well tolerated by patients, including after irradiation for cancer therapy (26, 28).

In this study, we have examined the lungs from rats that survived acute radiation pneumonitis, as granulomatous changes are a delayed injury (late effect). In our model, all rats receiving doses of 5 and 10 Gy, but not doses of 12 and 13 Gy, survived pneumonitis (10, 15, 19). With doses higher than 13 Gy (e.g., 15 Gy) no rats survived (19, 21, 30) long enough for investigation of late effects. We therefore focused on rats injured with 5–13 Gy irradiation to the thorax. At 13 Gy irradiation, 60–80% of the rats were lost to pneumonitis between 42–80 days. However, once they were past that phase they survived beyond 200 days (10, 30) to manifest late effects. Between 20 to 75% of the rats irradiated with radiation doses of 13 Gy with different doses and schedules of enalapril were protected during pneumonitis. The mitigation of late effects we observed with enalapril may be underestimated, since we did not account for the higher rate of attrition in the group irradiated with doses of 13 Gy alone, which lost more rats to severe and fatal pneumonitis.

Cholesterol clefts are empty spaces left by cholesterol crystals that are dissolved during tissue processing such as paraffin embedding and deparafinization. They have been described in many organs from different species, such as dog brain (31), mouse aorta (32), periapical lesions in human jawbone (33) and coronary artery of humans and pigs (34). Cholesterol granulomata in the lung have been reported in patients with pulmonary-associated pathologies, e.g., in lungs of heavy cigarette smokers (35), pulmonary arterial hypertension (36) and nonspecific interstitial pneumonia/fibrosis (37). Nodules have been described on computed tomography (CT) chest scans of patients (36), which may represent the large coalesced lesions we observed on histology. Barkhordari *et al.* characterized granulomas from lungs of nonspecific interstitial pneumonia patients (24). Their findings were similar to ours showing mono- and multinucleated giant cells with anti-CD68 antibody. They also observed strong staining of type II pneumocytes and cholesterol cleft granuloma lining cells. Granulomas have also been reported in patients after irradiation. Resected lung tissue from non-small-cell lung cancer patients treated with radiotherapy and investigated for therapy-associated tumor regression had cholesterol clefts that were at times associated with giant cells (38). The clinical significance for the lesions within the lung is not clear and will be an interesting topic for future investigation.

Travis *et al.* described cholesterol cleft-associated foci in C3H mouse lungs after single and fractionated doses of whole-thorax irradiation (9, 11, 12). These nodules were not characterized by cell type or quantified by time or dose after irradiation, as done in this study. However, they were reported to be the most striking changes in the irradiated lungs of the mice at 64 weeks (12). They were shown to occur with radiation doses >8 Gy and at

dose rates ranging from 0.01–8.8 Gy/min. Lymphoid accumulation in the alveolar lumina was observed (11) in addition to the foamy cells, cholesterol clefts and collagen accumulation. Our results in rats are very similar, although we did not observe significant lymphoid accumulation. Also, the increase in collagen in our study was not limited to these foci as reported in the mouse (9). In another study terminated at 76 weeks that used the same strain of rats as in this study, “granulomatous pneumonia” by cholesterol clefts were described after irradiation along with fibrosis that was not lethal (13).

Mechanisms for development of the cholesterol granulomas in the lung are not well described. Some investigators postulate that they result from recurrent pulmonary hemorrhage (36, 39). We did not observe evidence for hemorrhage in the irradiated lung sections we examined. Others relate them to the degradation of excess surfactant into phospholipids and cholesterol crystals that are then embedded in the surrounding tissue (40). Cholesterol (3%) is present in lipid extracts of bovine pulmonary surfactant (24, 41). More recently, pathways in phagocytic cellular metabolism have been studied, with a focus on the digestion of ingested apoptotic cells (42). In these studies, the phosphotidyl serine that is externalized on apoptotic cells activate peroxisomes proliferator-activated receptors (PPARs) and liver X receptors (LXRs) in phagocytes to mediate cholesterol efflux. This process fits best with our observations of giant cells and macrophages associated with the alveolar lesions and the cholesterol clefts in irradiated lungs. Apoptotic cells would be expected to increase in number in the lung after irradiation and attract macrophages. Phagocytosis of these cells would induce formation of cholesterol granules (as described for ingested apoptotic cells), which are then packed into clefts.

Mitigation by ACE inhibitors could also be explained by this mechanism, since the renin-angiotensin system has been reported to be involved in both apoptosis as well as in inflammation by macrophages. The ACE-inhibitor captopril completely abrogated apoptotic indices based on morphology, DNA fragmentation, and inducible caspase 1 and caspase 3 activities, in Fas-induced programmed death of human lung epithelial cells in culture (43). Bleomycin-induced apoptosis of cultured rat pulmonary epithelial cells was inhibited 91% by captopril or 82%, respectively, by neutralizing antibodies specific for angiotensin II (both $P < 0.01$) (44). In addition, observations in experimental animals show that alveolar macrophages initiated systemic inflammatory response (45). The inflammatory cascade included activation of the local renin-angiotensin system. In fact, macrophages expressed markers of the renin-angiotensin system (46). So inhibition of ACE with enalapril might be expected to reduce apoptosis, inflammation and the development of the alveolar lesions we observed.

We identified several indices of pulmonary dysfunction in rats surviving beyond 30 weeks after radiation doses of 5–13 Gy to the thorax, the lungs of which exhibited variation in cholesterol cleft numbers. We observed abnormalities in lung structure and function accompanying the increased density of alveolar lesions. However, a causal relationship between cholesterol clefts and dysfunction cannot be assumed. Cholesterol clefts also present in other pathological conditions affecting the lung. Future studies are needed for a better understanding of the mechanism and consequence of these lesions, or to reveal if they are related to recently described epithelial-to-mesenchymal transitions (47).

In summary, irradiation of the lung resulted in late developing granulomatous alveolar lesions that are associated with giant cells and cholesterol clefts. These injuries were observed in one strain of mouse (C3H), one strain of rat (WAG/RijCmcr) and in human lungs. In rats they began to appear around 21 weeks, after radiation pneumonitis had resolved and before fibrosis was readily detected. The foci increased in numbers with time, indicating a dynamic and ongoing injury. They also occurred earlier with higher doses of

radiation. Because they are easily detected by histology, which is the gold standard to monitor lung injury, they may serve as a convenient early marker of late radiation injury to the lung and to test countermeasures. Future studies are needed to determine if similar to radiation fibrosis, development of these lesions is regulated by genetic factors. Finally, we show here that enalapril is a mitigator of formation of pulmonary cholesterol clefts induced by radiation if started after 1 week or even after 20 weeks. This ACE inhibitor also mitigates radiation pneumonitis and pulmonary fibrosis (10).

Acknowledgments

This work was funded by NIH/NIAID RC-1 AI 81294, agreement U19 AI67734 and the Department of Radiation Oncology (MCW). We thank Merck Inc. for providing enalapril as a gift. Special thanks go to Qingping Wu (Department of Radiation Oncology) for assaying parameters of lung injury, Christine Duris from the CRI/MCW Histology Core and Carol Ann Bobrowitz from the Physiology Histology laboratory for immunohistochemistry, Marylou Mäder and Krista Paffenroth from the Department of Radiation Oncology for conducting irradiation and animal care and Stephanie Gruenloh from the Cardiovascular Center for the morphometric comparisons of Masson's trichrome stained sections.

References

1. Coggle JE, Lambert BE, Moores SR. Radiation effects in the lung. Environ Health Perspect. 1986; 70:261–91. [PubMed: 3549278]
2. Siemann DW, Hill RP, Penney DP. Early and late pulmonary toxicity in mice evaluated 180 and 420 days following localized lung irradiation. Radiat Res. 1982; 89(2):396–407. [PubMed: 7063621]
3. Robbins ME, Brunso-Bechtold JK, Peiffer AM, Tsien CI, Bailey JE, Marks LB. Imaging radiation-induced normal tissue injury. Radiat Res. 2012; 177(4):449–66. [PubMed: 22348250]
4. Mahmood J, Jelveh S, Calveley V, Zaidi A, Doctrow SR, Hill RP. Mitigation of radiation-induced lung injury by genistein and EUK-207. Int J Radiat Biol. 2011; 87(8):889–901. [PubMed: 21675818]
5. Jackson IL, Vujaskovic Z, Down JD. Revisiting strain-related differences in radiation sensitivity of the mouse lung: recognizing and avoiding the confounding effects of pleural effusions. Radiat Res. 2010; 173(1):10–20. [PubMed: 20041755]
6. Jackson IL, Vujaskovic Z, Down JD. A further comparison of pathologies after thoracic irradiation among different mouse strains: finding the best preclinical model for evaluating therapies directed against radiation-induced lung damage. Radiat Res. 2011; 175(4):510–8. [PubMed: 21338245]
7. Travis EL. Genetic susceptibility to late normal tissue injury. Semin Radiat Oncol. 2007; 17(2):149–55. [PubMed: 17395045]
8. Williams JP, Brown SL, Georges GE, Hauer-Jensen M, Hill RP, Huser AK, et al. Animal models for medical countermeasures to radiation exposure. Radiat Res. 2010; 173(4):557–78. [PubMed: 20334528]
9. Travis EL, Meistrich ML, Finch-Neimeyer MV, Watkins TL, Kiss I. Late functional and biochemical changes in mouse lung after irradiation: differential effects of WR-2721. Radiat Res. 1985; 103(2):219–31. [PubMed: 2991972]
10. Kma L, Gao F, Fish BL, Moulder JE, Jacobs ER, Medhora M. Angiotensin converting enzyme inhibitors mitigate collagen synthesis induced by a single dose of radiation to the whole thorax. J Radiat Res (Tokyo). 2012; 53(1):10–7. [PubMed: 22302041]
11. Travis EL, Peters LJ, McNeill J, Thames HD Jr, Karolis C. Effect of dose-rate on total body irradiation: lethality and pathologic findings. Radiother Oncol. 1985; 4(4):341–51. [PubMed: 3909241]
12. Travis EL, Bucci L, Fang MZ. Residual damage in mouse lungs at long intervals after cyclophosphamide treatment. Cancer Res. 1990; 50(7):2139–45. [PubMed: 2317805]
13. van Rongen E, Tan CH, Durham SK. Late functional, biochemical and histological changes in the rat lung after fractionated irradiation to the whole thorax. Radiother Oncol. 1987; 10(3):231–46. [PubMed: 3432599]

14. Molteni A, Moulder JE, Cohen EF, Ward WF, Fish BL, Taylor JM, et al. Control of radiation-induced pneumopathy and lung fibrosis by angiotensin-converting enzyme inhibitors and an angiotensin II type 1 receptor blocker. Int J Radiat Biol. 2000; 76(4):523–32. [PubMed: 10815633]
15. Zhang R, Ghosh SN, Zhu D, North PE, Fish BL, Morrow NV, et al. Structural and functional alterations in the rat lung following whole thoracic irradiation with moderate doses: injury and recovery. Int J Radiat Biol. 2008; 84(6):487–97. [PubMed: 18470747]
16. Gao F, Fish BL, Szabo A, Doctrow SR, Kma L, Molthen RC, et al. Short-term treatment with a SOD/catalase mimetic, EUK-207, mitigates pneumonitis and fibrosis after single-dose total-body or whole-thoracic irradiation. Radiat Res. 2012; 178(5):468–80. [PubMed: 23020094]
17. Sarkisova K, van Luijtelaar G. The WAG/Rij strain: a genetic animal model of absence epilepsy with comorbidity of depression (corrected). Prog Neuropsychopharmacol Biol Psychiat. 2011; 35(4):854–76.
18. Molteni A, Wolfe LF, Ward WF, Ts'ao CH, Molteni LB, Veno P, et al. Effect of an angiotensin II receptor blocker and two angiotensin converting enzyme inhibitors on transforming growth factor-beta (TGF-beta) and alpha-actomyosin (alpha SMA), important mediators of radiation-induced pneumopathy and lung fibrosis. Curr Pharm Des. 2007; 13(13):1307–16. [PubMed: 17506716]
19. Ghosh SN, Zhang R, Fish BL, Semenenko VA, Li XA, Moulder JE, et al. Renin-angiotensin system suppression mitigates experimental radiation pneumonitis. Int J Radiat Oncol Biol Phys. 2009; 75(5):1528–36. [PubMed: 19931735]
20. Kagaya Y, Hajjar RJ, Gwathmey JK, Barry WH, Lorell BH. Long-term angiotensin-converting enzyme inhibition with fosinopril improves depressed responsiveness to Ca2+ in myocytes from aortic-banded rats. Circulation. 1996; 94(11):2915–22. [PubMed: 8941121]
21. Szabo S, Ghosh SN, Fish BL, Bodiga S, Tomic R, Kumar G, et al. Cellular inflammatory infiltrate in pneumonitis induced by a single moderate dose of thoracic x radiation in rats. Radiat Res. 2010; 173(4):545–56. [PubMed: 20334527]
22. Ghosh SN, Wu Q, Mader M, Fish BL, Moulder JE, Jacobs ER, et al. Vascular injury after whole thoracic x-ray irradiation in the rat. Int J Radiat Oncol Biol Phys. 2009; 74(1):192–9. [PubMed: 19362237]
23. Bartlett MS. The square root transformation in analysis of variance. J Royal Statis Soc. 1936; 3(1): 68–78.
24. Barkhordari A, Stoddart RW, McClure SF, McClure J. Immunohistochemistry of cholesterol cleft granulomas in non-specific interstitial pneumonia. Pakistan J Biol Sci. 2005; 8(10):1383–6.
25. Robbins ME, Zhao W, Garcia-Espinosa MA, Diz DI. Renin-angiotensin system blockers and modulation of radiation-induced brain injury. Curr Drug Targets. 2010; 11(11):1413–22. [PubMed: 20583976]
26. Cohen EP, Bedi M, Irving AA, Jacobs E, Tomic R, Klein J, et al. Mitigation of late renal and pulmonary injury after hematopoietic stem cell transplantation. Int J Radiat Oncol Biol Phys. 2012; 83(1):292–6. [PubMed: 22104363]
27. Ward WF, Kim YT, Molteni A, Solliday NH. Radiation-induced pulmonary endothelial dysfunction in rats: modification by an inhibitor of angiotensin converting enzyme. Int J Radiat Oncol Biol Phys. 1988; 15(1):135–40. [PubMed: 3292488]
28. Kharofa J, Cohen EP, Tomic R, Xiang Q, Gore E. Decreased risk of radiation pneumonitis with incidental concurrent use of angiotensin-converting enzyme inhibitors and thoracic radiation therapy. Int J Radiat Oncol Biol Phys. 2012
29. Jenrow KA, Brown SL, Liu J, Kolozsvary A, Lapanowski K, Kim JH. Ramipril mitigates radiation-induced impairment of neurogenesis in the rat dentate gyrus. Radiat Oncol. 2010; 5:6. [PubMed: 20122169]
30. Medhora M, Gao F, Fish BL, Jacobs ER, Moulder JE, Szabo A. Dose-modifying factor for captopril for mitigation of radiation injury to normal lung. J Radiat Res. 2012; 53(4):633–40. [PubMed: 22843631]
31. Cramer SD, Miller AD, Medici EL, Brunker JD, Ritchey JW. Sellar xanthogranuloma in a dog. J Vet Diagnos Invest. 2011; 23(2):387–90.

32. Boesten LS, Zadelaar AS, van Nieuwkoop A, Hu L, Teunisse AF, Jochemsen AG, et al. Macrophage p53 controls macrophage death in atherosclerotic lesions of apolipoprotein E deficient mice. Atherosclerosis. 2009; 207(2):399–404. [PubMed: 19608184]
33. Lin HP, Chen HM, Yu CH, Kuo RC, Kuo YS, Wang YP. Clinicopathological study of 252 jaw bone periapical lesions from a private pathology laboratory. J Formos Med Assoc. 2010; 109(11): 810–8. [PubMed: 21126653]
34. Virmani R, Farb A, Carter AJ, Jones RM. Pathology of radiation-induced coronary artery disease in human and pig. Cardiovasc Radiat Med. 1999; 1(1):98–101. [PubMed: 11272363]
35. Corrin B, Soliman SS. Cholesterol in the lungs of heavy cigarette smokers. Thorax. 1978; 33(5): 565–8. [PubMed: 725824]
36. Nolan RL, McAdams HP, Sporn TA, Roggli VL, Tapson VF, Goodman PC. Pulmonary cholesterol granulomas in patients with pulmonary artery hypertension: chest radiographic and CT findings. AJR Am J Roentgenol. 1999; 172(5):1317–9. [PubMed: 10227509]
37. Cottin V, Donsbeck AV, Revel D, Loire R, Cordier JF. Nonspecific interstitial pneumonia. Individualization of a clinico-pathologic entity in a series of 12 patients. Am J Respir Crit Care Med. 1998; 158(4):1286–93. [PubMed: 9769293]
38. Junker K, Thomas M, Schulmann K, Klinke F, Bosse U, Muller KM. Tumour regression in non-small-cell lung cancer following neoadjuvant therapy. Histological assessment. J Cancer Res Clin Oncol. 1997; 123(9):469–77. [PubMed: 9341895]
39. Caslin AW, Heath D, Madden B, Yacoub M, Gosney JR, Smith P. The histopathology of 36 cases of plexogenic pulmonary arteriopathy. Histopathology. 1990; 16(1):9–19. [PubMed: 2307421]
40. Fisher M, Roggli V, Merten D, Mulvihill D, Spock A. Coexisting endogenous lipoid pneumonia, cholesterol granulomas, and pulmonary alveolar proteinosis in a pediatric population: a clinical, radiographic, and pathologic correlation. Pediat Pathol. 1992; 12(3):365–83.
41. McNally AK, Anderson JM. Interleukin-4 induces foreign body giant cells from human monocytes/macrophages. Differential lymphokine regulation of macrophage fusion leads to morphological variants of multinucleated giant cells. Am J Pathol. 1995; 147(5):1487–99. [PubMed: 7485411]
42. Han CZ, Ravichandran KS. Metabolic connections during apoptotic cell engulfment. Cell. 2011; 147(7):1442–5. [PubMed: 22196723]
43. Uhal BD, Gidea C, Bargout R, Bifero A, Ibarra-Sunga O, Papp M, et al. Captopril inhibits apoptosis in human lung epithelial cells: a potential antifibrotic mechanism. Am J Physiol. 1998; 275(5 Pt 1):L1013–7. [PubMed: 9815121]
44. Li X, Zhang H, Soledad-Conrad V, Zhuang J, Uhal BD. Bleomycin-induced apoptosis of alveolar epithelial cells requires angiotensin synthesis de novo. Am J Physiol Lung Cell Mol Physiol. 2003; 284(3):L501–7. [PubMed: 12573988]
45. Chao J, Wood JG, Gonzalez NC. Alveolar hypoxia, alveolar macrophages, and systemic inflammation. Respir Res. 2009; 10:54. [PubMed: 19545431]
46. Veerappan A, Reid AC, Estephan R, O'Connor N, Thadani-Mulero M, Salazar-Rodriguez M, et al. Mast cell renin and a local renin-angiotensin system in the airway: role in bronchoconstriction. Proc Natl Acad Sci U S A. 2008; 105(4):1315–20. [PubMed: 18202178]
47. Nagarajan D, Melo T, Deng Z, Almeida C, Zhao W. ERK/ GSK3beta/snail signaling mediates radiation-induced alveolar epithelial-to-mesenchymal transition. Free Radic Biol Med. 2012; 52(6):983–9. [PubMed: 22198183]

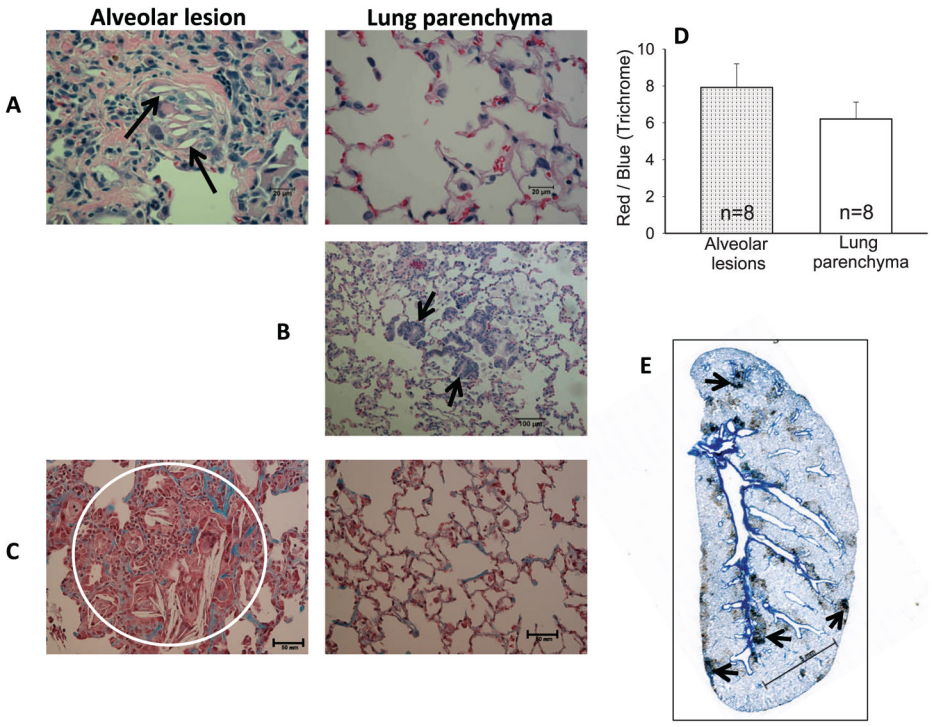

FIG. 1.

Histology. Representative images from typical alveolar lesions (left) and lung parenchyma (right) are shown after (panel A) H&E staining with arrows pointing to empty cholesterol clefts. Panel B: H&E stained section of lung parenchyma with typical epithelial cell metaplasia (see arrows). Panel C: Trichrome stained section with a circle enclosing an alveolar lesion that was analyzed for morphometric comparisons of the ratio of red (noncollagenous):blue (collagen) staining. Panel D: Graphical representation of red:blue ratio in alveolar lesions (dotted bar) and lung parenchyma (open bar). Values are presented as mean ± SEM. *n* = number of rats per group. There was no statistically significant difference in the red:blue stain ratio between these 2 groups. Panel E: Whole-mount lung section immunostained with anti-CD 68 antibody under low magnification. Arrows point to islands of positively stained macrophages. Bars represent 20 μm in panel A, 100 μm in panel B, 50 μm in panel C and 5 mm in panel E.

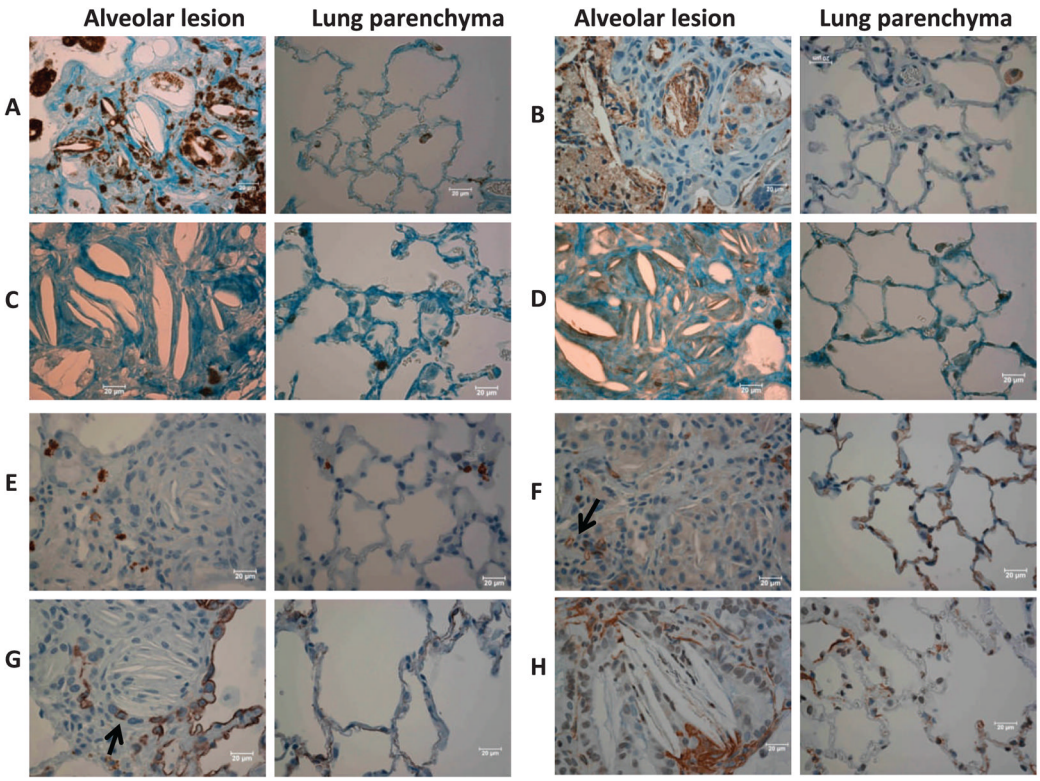

FIG. 2.

Immunohistochemistry. Representative images from typical alveolar lesions (left) and lung parenchyma (right) immunostained with antibodies from irradiated rats as follows, panel A: CD 68 (macrophages), panel B: myeloperoxidase (macrophages and neutrophils), panel C: CD 43 (T cells), panel D: CD 79a (B cells), panel E: tryptase (mast cells), panel F: CD 31 (vascular endothelial cells), panel G: keratin-7 (epithelial cells) and panel H: smooth muscle alpha actin (smooth muscle cells). Bars represent 20 μm. Note macrophages stained positive for CD-68 (panel A) and myeloperoxidase (panel B) appear more abundant in alveolar lesions compared to the parenchyma, highlighting areas that are clearly visible in the whole-mount section in Fig. 1E. Arrows in panels F and G point to a narrowed blood vessels and airway, respectively.

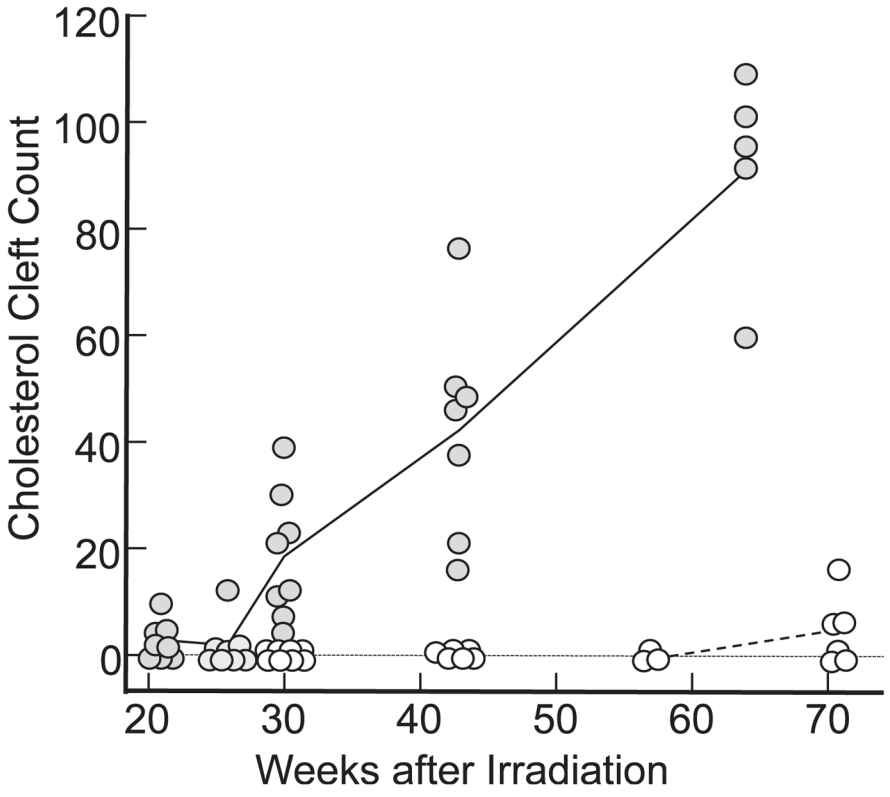

FIG. 3.

Scatter plots of cholesterol cleft counts/whole-mount lung sections. Open circles represent unirradiated (control) rats corresponding to 30 (n = 8), 43 (n = 6), 57 (n = 3) and 71 (n = 6) weeks after irradiation in the irradiated groups. No cholesterol clefts were observed before 71 weeks in these rats. Closed circles represent clefts at 21 (n = 8), 25 (n = 8), 30 (n = 8), 43 (n = 7) and 64 (n = 5) weeks after a radiation dose of 13 Gy. All points positioned exactly on the vertical axis, except for some zero values shown below zero for clarity. The solid black (13 Gy) and dashed gray (0 Gy) lines connect mean values in each group.

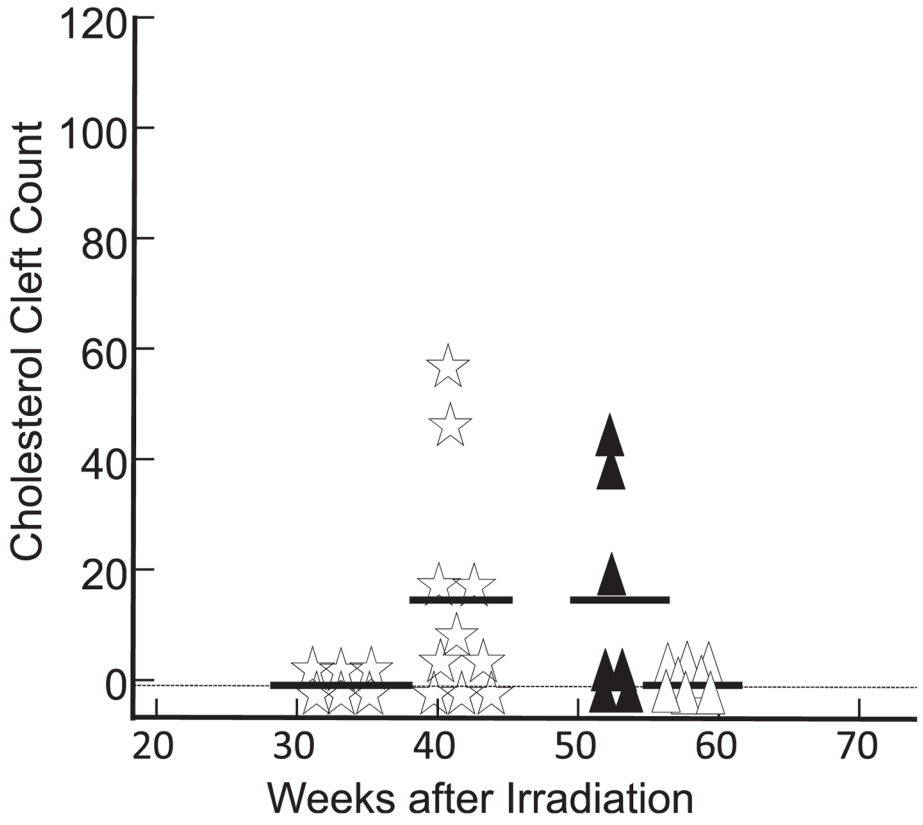

FIG. 4.

Scatter plots of cholesterol cleft counts/whole-mount lung sections. Open triangles represent results from lungs of rats ($n = 8$) after 56 weeks after irradiation with 5 Gy to the thorax. Solid black triangles represent results from lungs ($n = 7$) after 53 weeks after irradiation with 10 Gy to the thorax. Open stars represent results from lungs after 33 weeks ($n = 6$) and 41 weeks ($n = 10$) after irradiation with 12 Gy to the thorax. No cholesterol clefts were observed after a radiation dose of 5 Gy at 56 weeks or 12 Gy at 33 weeks. All points positioned exactly on the vertical axis, except for some zero values shown below zero for clarity. The line in each group represents the mean value.

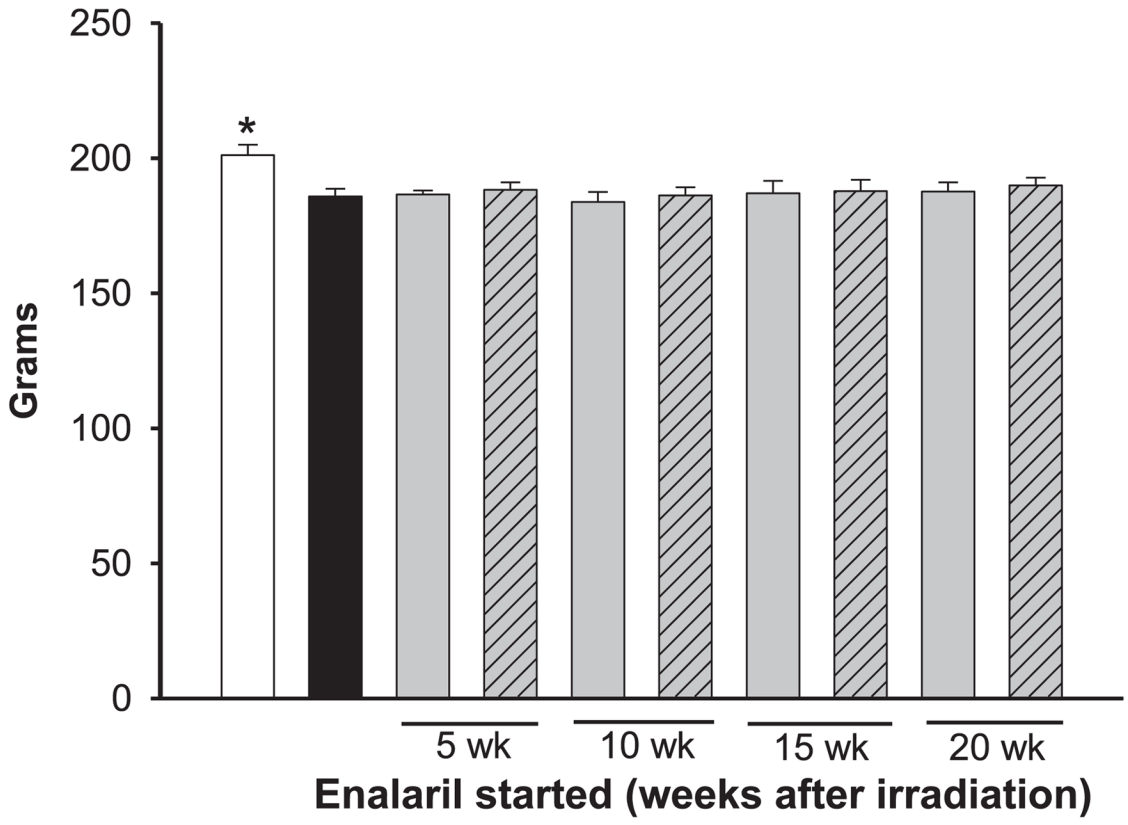

FIG. 5.

Graph showing mean ± SEM body weights of rats in grams at 30 weeks after irradiation. Open bar represents unirradiated (control) rats ($n = 8$). Solid black bar represents rats with radiation doses of 13 Gy to the thorax ($n = 8$). Gray bars represent thorax-irradiated rats (13 Gy) given enalapril started at different times after irradiation, as labeled in the figure. Solid gray bars ($n = 8$) depict the weight of rats treated with 60 mg/L enalapril and hatched bars ($n = 8$) show the weight of rats treated with 30 mg/L enalapril. Unirradiated rats had higher body weight compared to all other groups ($*P < 0.05$, ANOVA with Holm-Sidak method). No difference was observed for results between the other groups.

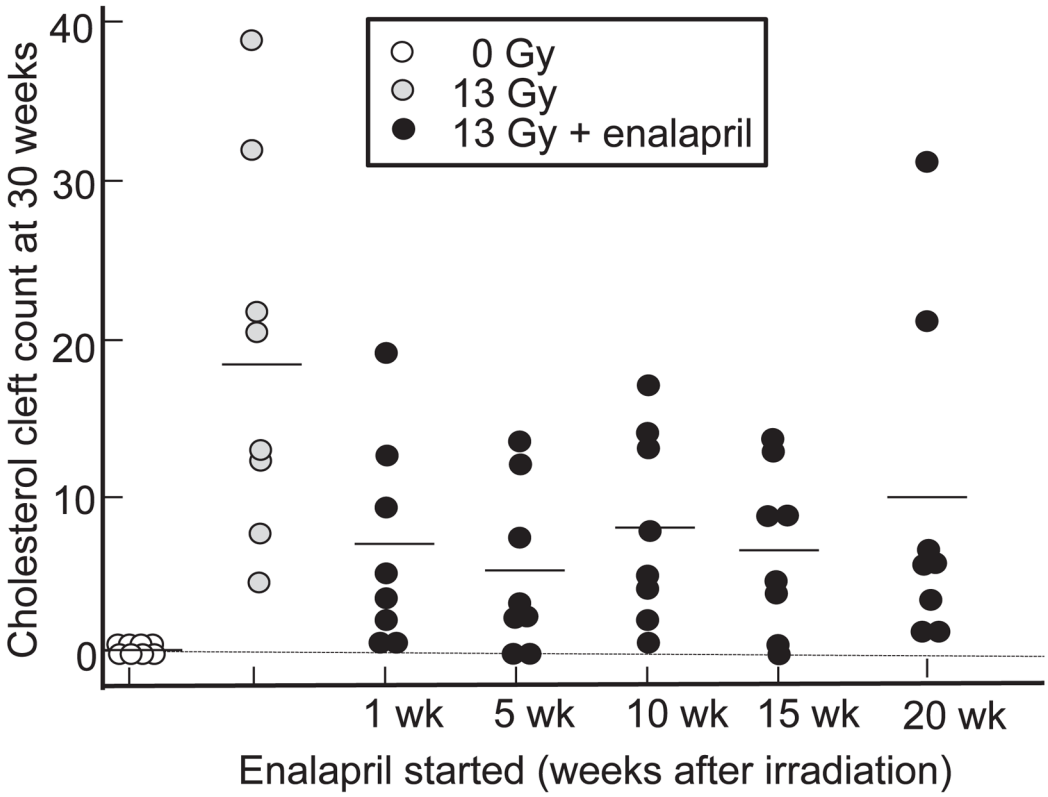

FIG. 6.

Scatter plots of cholesterol cleft counts at 30 weeks in unirradiated rats (open circles) and after 13 Gy irradiation to the whole thorax (gray circles). The black circles represent 13 Gy + enalapril 60 mg/L started at 1, 5, 10, 15, and 20 weeks after irradiation and continued to 30 weeks (210 days). $n = 8$ rats/group. The line in each group represents the mean value.

TABLE 1

Antibodies and Dilutions Used for Immunohistochemistry

Antibody	Dilution	Reactivity	Source
Myeloperoxidase	1:100	Neutrophil	Abcam no. ab9535
Tryptase	1:150	Mast cell	IMGENEX no. IMG-80250
CD 31	1:200	Endothelial cell	BD Pharmingen no. 555025
Keratin-7	1:25	Epithelial cell	Cell Signaling Technology no. 4898s
Actin	1:100	Smooth muscle cell	Dako no. M0851
CD 68	1:400	Macrophage	abD Serotec no. MCA341R
CD 43	1:175	T Lymphocyte	Abcam no. ab22351
CD 79a	1:200	B Lymphocyte	Abcam no. ab3121

TABLE 2

Summary of Results from Rats Irradiated With 5, 10 or 13 Gy to The Thorax

			Functional analysis (at the time of cholesterol cleft count)							
Whole thoracic irradiation (Gy)	**Weeks after irradiation**	**Average no. of cholesterol cleft/ whole mount section**	**Breathing rate**	**Body weight**	**Lung collagen**	**Total lung ACE activity**	**Right ventricular hypertrophy**	**Pulmonary vascular resistance**	**Dry lung weight**	**Arterial distensibility**
5	56	0	N/A[d]	± (22)	N/A	↓(22)	± (22)	± (22)	± (22)	± (22)
10	53	14	±[a] (15)	↓([c] (22)	N/A	↓(22)	± (22)	± (22)	↑ (22)	↓(22)
13	30	19	↑[b] (10)	↓(	↑(10, 16)	↓(	↑	↑	↑	↓(

[a] No significant change.

[b] Significantly increases compared with age-matched controls.

[c] Significantly decreases compared with age-matched controls

[d] Data not available.